Quantification of mechanofluorochromism at the macroscale via colorimetric analysis of controlled mechanical stimulation

Benjamin Poggi, Laurence Bodelot, Marine Louis, Rémi Métivier, Clémence Allain

ARTICLE

Quantification of mechanofluorochromism at the macroscale via colorimetric analysis of controlled mechanical stimulation

Received 00th January 20xx,
Accepted 00th January 20xx

DOI: 10.1039/x0xx00000x

Benjamin Poggi, [a] Laurence Bodelot, *[b] Marine Louis, †[a] Rémi Métivier *[a] and Clémence Allain *[a]

The use of mechanofluorochromic (MFC) molecular materials as mechanical stress probes is challenging since quantitative studies of this phenomenon remain rare. The most common approach to quantify the fluorescence response of MFC materials involves a diamond anvil cell. However, this requires high isotropic pressures, which are far from ordinary conditions. We report here the design of a setup able to apply anisotropic mechanical stimuli such as pure unidirectional compression and shear stress, both controlled in intensity. A well-known MFC compound, **DFB-H**, was submitted to pure compression or shearing while simultaneously recording fluorescence movies. **DFB-H** crystals were found to be responsive to both types of stimuli but subsequent data analysis revealed higher sensitivity to shearing than to pure compression. Indeed, fluorescence colour change was detected by colorimetric analysis and linked to the intensity of applied force to estimate a threshold. **DFB-H** MFC response was observed for pressures in the order of tens of MPa whereas only few kPa were enough to induce MFC response by shearing. This novel setup, combined with a colorimetric analysis, is a promising approach for quantification of MFC response at the macroscale and for future development of mechanical stress probes.

Introduction

Luminescent materials sensitive to external stimuli are an emerging class of smart materials due to their potential applications in optical sensors and devices. [1,2] Among them, mechanofluorochromic (MFC) materials exhibit a modification of their fluorescence properties upon an external mechanical stimulus (grinding, bending, shearing…). [3] This phenomenon is generally attributed to changes in molecular packing and can be reversible either spontaneously at room temperature or upon specific action such as heating or solvent fuming. [4] Thus, the possibility to follow fluorescence modifications by non-invasive spectroscopic measurements makes them good candidates for mechanical stress probes. [5] Such mechanosensors can be used for surface mapping, [6] mechanical printing, [7] anticounterfeiting [8] and data storage [9–11]. In addition to organic conjugated molecules [12] and metal coordination complexes, [13] MFC polymers [14] and polymer composites [15] have also been developed.

Most of the time, MFC response is evidenced only qualitatively by grinding the molecules obtained as powder into a mortar. However, to design efficient sensors based on these materials, it is crucial to quantify their response to mechanical stimulation. As a result, the force applied on the sensor can be deduced from its modification of fluorescence colour or intensity. Recently, quantitative studies of MFC behaviour have been performed at the nanoscale through atomic force microscopy (AFM) on polydiacetylene (PDA) thin films [16] and Pt(II) complex [10] crystals, as well as difluoroboron β-diketonate complex [17] and conjugated polymer nanoparticles. [18,19] These studies have shown that forces ranging from nN to µN are required to induce morphological modifications responsible for the fluorescence response. Concerning PDA, a correlation between force and fluorescence intensity has even been evidenced. [16] On the other hand, MFC phenomenon has also been investigated at the macroscale by applying hydrostatic pressure to molecular materials using a diamond anvil cell (DAC) setup. This technique is widely used to get insights into the mechanisms that govern MFC behaviour thanks to its potential for coupling with in situ characterizations (Raman scattering, [20,21] IR, [22] X-ray diffraction, [22–24] UV-visible absorption [21,22] and fluorescence spectroscopy [20–24]). [25] In DAC, MFC response is caused by pressures ranging from hundreds of MPa to tens of GPa depending on the system. [20–26] However, a given compound sometimes exhibits either enhanced [20] or opposite [27] fluorescence spectra shifts when submitted to DAC experiment compared to mortar grinding. These different behaviours may be driven by the nature of the mechanical stimuli: the first one being an isotropic compression while the second is an anisotropic pressure coupled with a shear stress. Studies where MFC compounds are submitted to unidirectional compression manually, [28] via hydraulic press [29,30] or indentation [6] reveal that stresses in the order of MPa to tens of MPa are required to observe MFC response. Sagawa *et al.* have attempted to semi-quantitatively estimate the fluorescence change triggered by spatula scratching with a force gauge. [31] Nevertheless, to the best of our knowledge, no other quantitative study of the fluorescence response to anisotropic force has been reported at the macroscale since the aforementioned examples.

[a] *Université Paris-Saclay, ENS Paris-Saclay, CNRS, PPSM, 91190, Gif-sur-Yvette, France*
[b] *LMS, CNRS, École Polytechnique, Institut Polytechnique de Paris, Route de Saclay, 91128 Palaiseau Cedex, France*
[c] *Address here.*
† Current address: Graduate School of Materials Science, Nara Institute of Science and Technology, 8916-5 Takayama, Ikoma, Nara, Japan
Electronic Supplementary Information (ESI) available: experimental conditions for all the samples, data processing details and pictures of shearing experiments on impregnated papers (PDF). A movie is also provided as supporting material. See DOI: 10.1039/x0xx00000x

Herein, we propose a new method to assess the type and intensity of force that has to be applied to a macroscopic powder of a difluoroboron β-diketonate complex (**DFB-H**) to observe an MFC response. These boron complexes are well known for their intense solid-state fluorescence as well as their polymorphism. [32,33] **DFB-H** was selected for this study because it shows a high fluorescence quantum yield in the solid state, and a large emission spectral shift upon mechanical stimulation. Its photophysical properties have been previously described by our group. [34] An instrumental setup able to apply either unidirectional compression or shearing in a quantitative manner while recording fluorescence images was designed for this purpose and allowed us to better understand the response of this compound to mechanical stimuli. We developed an automatic data processing method based on colorimetric analysis to enable the two-dimensional detection of fluorescence colour change as a function of applied mechanical stress. This strategy provided quantitative insights into the magnitude of unidirectional compression or shear force necessary to induce the MFC phenomenon for this compound.

Results and discussion

As-synthesized **DFB-H** (see structure in Figure 1A) powder emits a cyan blue fluorescence with a maximum emission at 458 nm. After grinding in a mortar, a yellow fluorescent powder is obtained with a maximum emission at 530 nm (Figure 1B, C). This large bathochromic shift of 2970 cm^{-1} corresponds to a crystalline to amorphous phase transition, as evidenced in a previous study of our group by PXRD data obtained before and after grinding the **DFB-H** powder. [34] However, using a mortar to manually grind MFC powders does not provide quantitative information on the intensity of the applied force. Furthermore, it does not allow concluding about the type of mechanical stimulation (compression or shearing) to which **DFB-H** is sensitive.

Hence, a specific setup was designed in order to apply a controlled mechanical stimulus to a powder sample while simultaneously observing its fluorescence response (Figure 2A). **DFB-H** crystals exhibiting blue fluorescence are deposited on a glass-window. A cylindrical pestle can apply either a vertical compression via a linear motor or a compression combined with a rotation resulting in a shearing thanks to an additional rotation motor. **DFB-H** powder is irradiated through the other side of the glass-window with a UV light at 365 nm. A CCD camera equipped with a lens allows to record fluorescence pictures (in RGB colour space) every two seconds by means of a mirror placed at 45° under the observation window. A sensor (load cell) located on top of the mechanical system records vertical force and torque values every second. Consequently, in the movie generated at the end of the experiment (Figure 2B, C, Supporting Movie S1), each fluorescence picture is associated with well-defined force and torque values. Both constant vertical force and compression ramp force experiments can be implemented with this setup while the pestle can also rotate. 41 tests were performed on **DFB-H** crystalline material, including 8 unidirectional pure compressions without rotation as listed in Table S1. The rest of the tests consists of shearing experiments: 9 compression ramps and 24 constant force experiments coupled with rotation. The complete list of compression ramps and constant force experiments are listed in Table S2. Figure 2B shows snapshots of a movie corresponding to a pure compression experiment. As expected, on the first picture, the deposited **DFB-H** crystal emits blue fluorescence before any force is applied. The crystal stays blue until t = 33 s but, when it is further compressed, the yellow amorphous phase appears in its center, indicating that **DFB-H** is sensitive to pure compression. In the case of the shearing experiment (Figure 2C), the pestle starts applying a compression ramp from 0 N to 70 N associated with a rotation starting from 20 N. Between 0 N and 20 N, no fluorescence colour change is observed. As soon as the rotation starts, the emissive material is spread on the substrate as shown in the pictures at 176 s and 350 s. More significantly, yellow fluorescence appears progressively along with the pestle rotation, meaning that **DFB-H** is sensitive to shear stress. Moreover, due to a shear intensity increasing with the pestle radius, the crystals located under the external area of the pestle turned yellow before the ones located at the center.

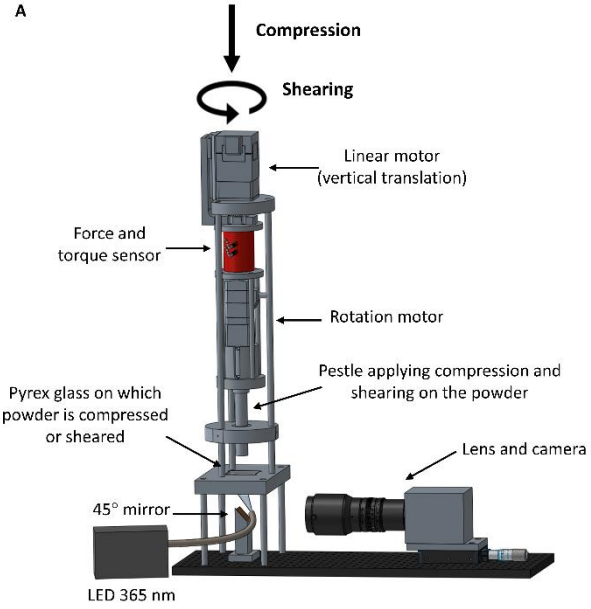

Fig. 2 (A) Schematic of the setup and first, middle and last frames of the movie for (B) a pure compression experiment and (C) a compression ramp experiment with rotation (shearing).

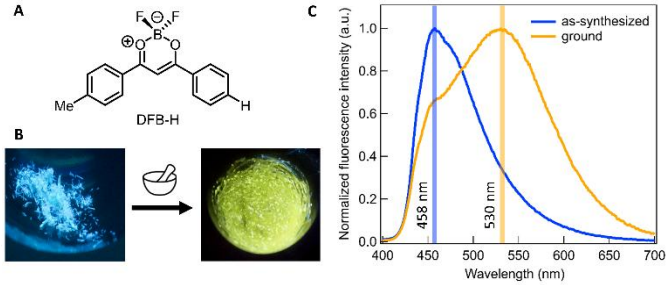

Fig. 1 (A) Structure of **DFB-H**, (B) pictures of **DFB-H** as synthesized powder (left) and ground powder (right) in a mortar and (C) corresponding normalized emission spectra (excitation at 365 nm).

Following these qualitative observations, **DFB-H** MFC response to pure compression and to shearing was further investigated in a quantitative manner via the detection of the fluorescence colour change in the pictures. Indeed, each pixel of the experimental movie that turns from blue to yellow fluorescence can be considered as transformed and then linked to a pressure or to a local shear value, given spatial position and measured force or torque value. For this purpose, dedicated automatized data processing was developed as follows (Figure S1). Raw experimental fluorescence movies are recorded in RGB colour space, but such coordinates are not suitable for discriminating the yellow fluorescence from the blue one. Hence, our approach consists in using the HSV (Hue, Saturation and Value) cylindrical colour space (Figure S2) derived from the RGB one by simple mathematical equations reported in SI (Section 3). The hue parameter represents the colour tone and can therefore be related to the emission wavelength, whereas saturation and value parameters express respectively purity and intensity of the colour. HSV colour space turns out to be a powerful tool for analytical studies such as pH [35] and ion [36,37] sensing, detection of plasmonic nanoparticles [38] and fluorescence measurements [39] including quantification of MFC response in a polymer matrix [40]. Inspired by the latter work, we tailored this strategy to our system: indeed, the main advantage of HSV colour space obviously lies in the fact that all colour information is included within a single parameter, or coordinate, H.

The data processing is divided in three main steps (Figure S1). The first one corresponds to the conversion of movie images from RGB to HSV colour space (after removal of the background, see details in SI Figure S3). The second step consists in determining a criterion on the H coordinate in order to distinguish the newly appearing yellow pixels from the blue ones. Histograms of H coordinates corresponding to all the fluorescent pixels of the first and last picture of the movie are plotted respectively in blue and yellow, as shown in Figure 3. According to the blue histogram, pixels from the first picture are characterized by a H coordinate centered around 0.61-0.62, which is consistent with blue colour in HSV colour space (Figure S4). Regarding the yellow histogram, it is worth noting that it shows a higher number of fluorescent pixels, which corresponds to the spreading of matter during the shearing experiment. More importantly, the new distribution is shifted toward lower values of H, corresponding to green colour in HSV colour space. This can also be noticed in the last image (bottom inset in Figure 3), where most of the pixels exhibit a greenish fluorescence. This is caused by the mixing of both blue and yellow **DFB-H** phases on the same pixel, as confirmed by colorimetric analysis of fully ground **DFB-H** (Figure S4). The change undergone by the yellow histogram, compared with the initial blue one, appears to be significant enough to enable the establishment of a reliable threshold conversion criterion on the H coordinates. This threshold H_C was defined as followed:

$$H_C = H_{avg} - 3\sigma \qquad (1)$$

with H_{avg} the mean H value of the blue histogram and σ the standard deviation. To exclude the vast majority of the blue pixels, a strong constraint was chosen with the 3σ parameter. Due to small differences including the amount of material deposited and lighting conditions, H_C slightly varies in each experiment and its value, determined in the range 0.561-0.593, is reported for each experiment in Tables S1 and S2. All pixels having a H coordinate below this threshold are detected by the code which then edits a binarized movie (Figure S1): non-black pixels (value 1) correspond to transformed yellow material, whereas the black ones (value 0) are either background or initial blue fluorescent **DFB-H**. This binarization facilitates the subsequent identification and counting of pixels that exhibit a fluorescence colour shift.

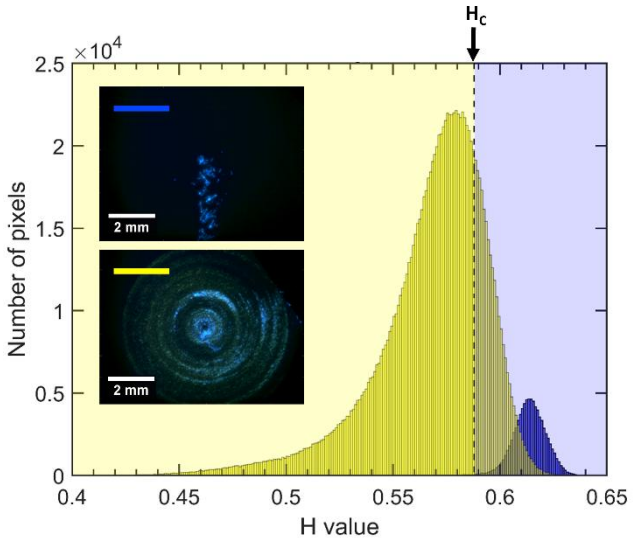

Fig. 3 Histograms of H coordinate for the first (top inset, blue) and last (bottom inset, yellow) pictures of the movie for experiment #14 (see Table S2).

In the case of the pure compression experiments, spreading of fluorescent material is limited. Hence, a threshold indicating the stress necessary to observe a marked MFC response can be readily identified using the ratio between the number of yellow fluorescent pixels and the total of fluorescent pixels (blue + yellow) as plotted against the stress applied to the crystal (Figure 4 and S5). At low stress values, this ratio slightly decreases due to a crushing of the crystal, (leading to a spread of the blue fluorescent material) and a concurrent ineffective conversion to the yellow phase. After this initial decrease, the ratio then steadily increases up to 20% suggesting effective MFC behaviour. The point at which the ratio starts increasing is thus defined as the threshold of MFC response. For the 8 pure compression experiments, this threshold corresponds to stresses between 13 and 281 MPa, which is in agreement with the order of magnitude reported in the literature for MFC response of other compounds [6,29,41,42]. While we cannot exclude that, on some of the tested crystals, the presence of defects lowers the stress threshold that triggers an MFC response, the dispersion of the observed threshold values can probably be largely explained by the fact that

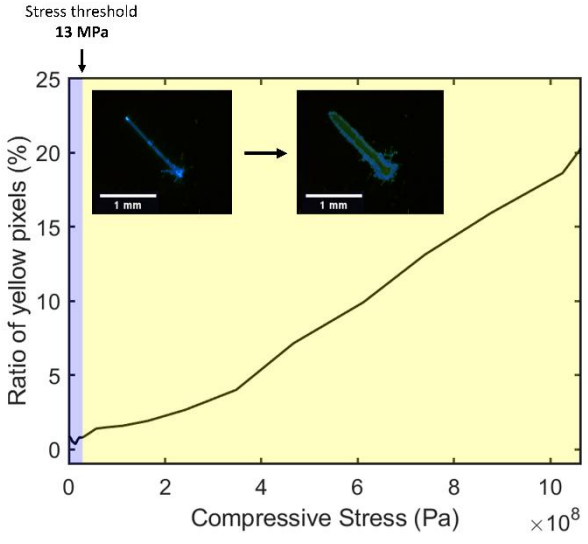

Fig. 4 Ratio of yellow pixels over total of fluorescent pixels (blue + yellow) against pure compressive stress for experiment #1 (see Table S1). The corresponding snapshots before (left) and after (right) compression are in inset.

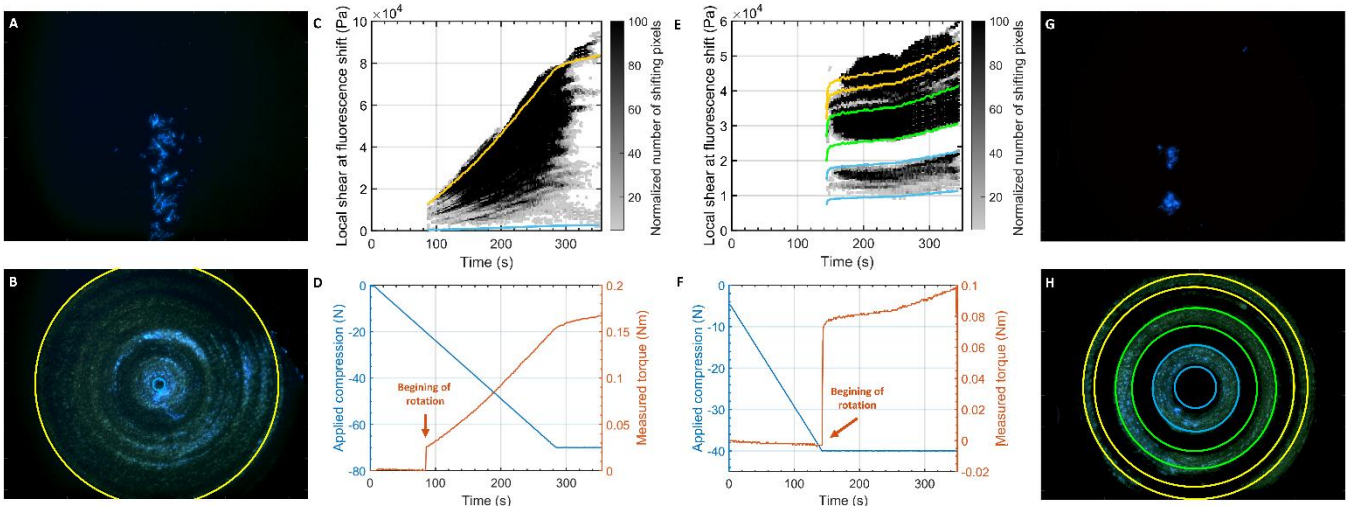

Fig. 5 (A, G) Initial and (B, H) final images of 2 movies, (C, E) plot of local shear at fluorescence shift and (D, F) corresponding applied compression and measured torque versus movie time for (left, A, B, C, D) a compression ramp (experiment #14) and (right, E, F, G, H) a constant compression experiment (experiment #36).

the **DFB-H** crystals are anisotropic, [34] which results in some of the crystalline faces being more sensitive to compression than others.

In the case of shearing experiments, the previous method cannot be applied because, contrary to compression, the local shear stress on a crystal depends on its position under the pestle. As a consequence, once the pixels that underwent an MFC response are detected, a third and final step consisting of linking them to the local shearing value they were submitted to is required. More precisely, on a given snapshot of the binarized movie, only the pixels that: (i) turned from black or blue to yellow and (ii) were not already detected as yellow in the previous snapshots are counted, and their spatial coordinates determined. For each pixel complying with these conditions, the shear stress that locally induced MFC response, F_N (in Pa), can be expressed as a function of the pixel distance to the pestle center r and measured torque C following equation (2) (see SI section 7 for details) below:

$$F_N(r) = r \times \frac{2C}{\pi R^4} \qquad (2)$$

with R the pestle radius.

Then, a graph summarizing all the local shearing values of yellow pixels appearing versus time of the movie is plotted (Figure 5C, E). For a given time (*i.e.*, snapshot), all the points represent pixels that shifted to yellow for a local shear stress readable on the y-axis. These graphs are distributions, meaning that black points correspond to a high number of pixels shifting to yellow, whereas grey points correspond to a low number of pixels shifting to yellow for a given local shear stress. As shown in Figure 5D and 5F, as soon as the pestle starts to rotate, the measured torque readily increases. Then, it either continues to increase linearly in the case of a compression ramp (Figure 5D) or it reaches a plateau as in the case of a constant applied vertical compression (Figure 5F). The compression ramp experiments allowed us to evaluate the range of applied vertical force needed to detect fluorescence change. Then, constant force experiments in this range were performed to determine a shearing threshold value.

In the example Figure 5A-D, when a compression ramp is applied to **DFB-H** powder while the pestle is rotating, MFC response is observed for local shear stresses between 0.2 kPa and 95 kPa depending on the position of the powder under the pestle and the vertical force applied. According to equation (2), the larger the circle radius is, the higher the locally applied shearing is. Black points at high (low) local shear stress are thus attributed to pixels changing from blue to yellow in the external (central) area of the pestle. Moreover, the local shear at which new yellow fluorescent pixels appear is increasing with time, which is consistent with the rise of the compression force intensity. Overall, for the 9 compression ramps performed with the pestle rotating, the local shear stress thresholds triggering MFC response are determined to be between 0.2 kPa and 10 kPa. No influence of the crystal size (Figure S7) on the shearing thresholds was observed, as evidenced in Table S2. Despite the fact that the threshold values are spanning a large range, they remain far below the stresses measured in pure compression (no rotation of the pestle). These values being measured systematically at the beginning of the compression ramps (low vertical forces), we decided to record a series of experiments combining rotation of the pestle with a constant applied compression, which results in a constant measured torque during the experiment. Typical snapshots of such an experiment are depicted in Figure 5G and 5H. In this experiment, the MFC response is induced by local shear stresses ranging from 9.3 kPa to 59.7 kPa, depending only on the position of the crystal under the pestle. Moreover, the points representing these pixels shifting to yellow are concentrated in different areas of given local shear ranges (blue, green and yellow lines) which can be assigned to different circular bands (or "donuts") of fluorescent material drawn respectively in the corresponding snapshot (Figure 5H).

All other constant force experiments (summarized in Table S2) exhibit a behaviour similar to the experiment described in Figure 5E-H. Although the distribution shape of local shear sometimes slightly varies owing to differences in powder initial deposition, the same tendencies are observed. In that way, the shearing thresholds derived from Figure 5E provided relevant information to quantify more precisely the MFC phenomenon for **DFB-H**. The shearing threshold was systematically defined as the lowest local applied shear at which a pixel was detected as yellow (Figure S8) and its values are reported in Table S2. This analysis yielded an order of magnitude of shearing stress required to observe the **DFB-H** MFC response, which lies between 0.03 kPa and 9.3 kPa. These thresholds are far below the ones determined for pure compression (in the order of MPa), indicating that **DFB-H** is much more sensitive to shearing than to pure compression. According to Krishna *et al.*, who performed nanoindentation studies on DFB avobenzone, applying an indentation with a certain angle to the molecular

planes induces better slipping between them than applying an indentation perpendicular to the crystal plane.[43,44] Thus, our results—that show a higher threshold in compression that in shearing—are consistent with their study of the mechanical properties of DFB derivatives.

To analyse further the dispersion of our results, we looked at the torque measured during these shearing experiments, which significantly varies from one experiment to another depending on the contact area between the **DFB-H** powder and the pestle. However, the torque measured remains almost constant during the whole experiment, meaning that the local shearing applied on a crystal is also constant and only depends on its position under the pestle. For the 24 constant force experiments, the shearing threshold was plotted against the torque value at the corresponding time (Figure 6). First, the plot exhibits a clear trend: the value of the shearing threshold increases along with the applied torque. Since the setup cannot apply torques lower than 0.002 Nm with good accuracy, the absolute shearing threshold at which **DFB-H** shows MFC may be below 0.03 kPa, which represents the intrinsic sensitivity of the MFC material to external shear stress.

Then, since we are interested to know the shearing stress to apply to obtain an MFC response that could be detected by the naked eye and taking into account that the torque varies from one experiment to another but remains constant during one given experiment, we looked at the amount of material transformed during one experiment. For this, the ratio of yellow pixels over the total number of fluorescent (yellow + blue) pixels was determined for the last snapshot of each experiment, similarly to the pure compression experiments (Table S2). By looking at the last snapshot and associated binarized picture of each experiment, we considered that MFC response is visually detectable when the final ratio of yellow pixels is at least 5 % (Figure S9C, D). Most of the experiments with a final ratio below 5 % (Figure 6, blue points) exhibit lower torque values and provide shearing thresholds between 0.03 and 4.6 kPa. In these low-torque experiments, although a few scattered pixels are detected as yellow (Figure S9B) MFC response is not perceptible to the naked eye when looking at the snapshots (Figure S9A). This low conversion rate from blue to yellow phase is likely due to an applied stress that is too small to induce the MFC transition for a large fraction of the material. In contrast, the majority of experiments with a final ratio higher than 5 % (Figure 6, red points) corresponds to higher values of torque and the corresponding shearing thresholds fall between 0.5 and 9.3 kPa. The dispersion of shearing threshold values could be due to variations in the amount of crystals deposited as well as in their shapes. Interestingly, the system shows good reversibility since the blue phase is recovered upon thermal annealing of the sheared sample (Figure S10). Moreover, subsequent shearing of the annealed sample gives a shearing threshold close to the one determined after the first stimulation (Table S3). Finally, with the perspective of using **DFB-H** as a mechanical sensor, it has been impregnated on cellulose paper as the host matrix (Figure S11). The resulting **DFB-H** impregnated papers exhibited MFC response to shearing applied with the setup and preliminary experiments revealed shearing threshold ranging from 0.04 to 0.5 kPa (Table S3). This study provides, for the first time, an order of magnitude of shearing required to observe the MFC response of **DFB-H** at the macroscale.

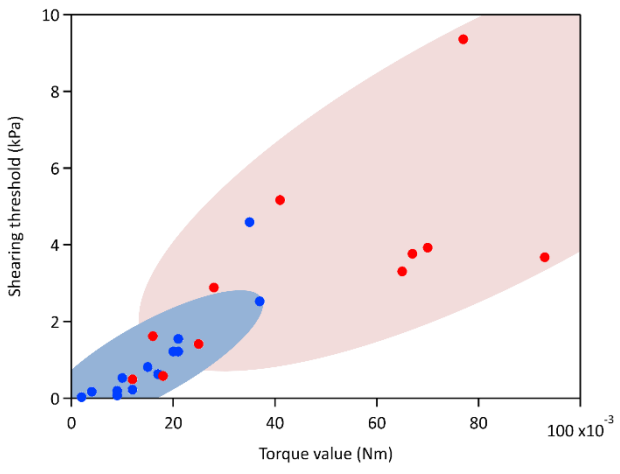

Fig. 6 Plot of shearing thresholds determined for each of the 24 constant force experiments versus the torque value at the corresponding time. Blue (red) markers correspond to experiments with a final ratio of yellow pixels over total (yellow + blue) pixels lower (respectively higher) than 5 %.

Conclusions

In this work, a setup able to apply an intensity-controlled (i) compression or (ii) shearing mechanical stress to an MFC compound, **DFB-H**, was designed in such a way that fluorescence colour change can be simultaneously probed. **DFB-H** crystals were submitted to either pure vertical compression or shearing (compression + rotation of the pestle), and turned out to be sensitive to both mechanical stimuli. To better understand the MFC behaviour of **DFB-H**, a complete data processing based on colorimetric analysis was developed to relate the detected fluorescence colour change to the applied stress. This quantitative analysis shows that **DFB-H** is responsive to compression of tens of MPa and to shearing in the order of kPa, thus evidencing a much higher sensitivity to shearing than to compression. Additionally, threshold values of the mechanical shearing stress necessary to allow the phase transition between the blue and the yellow phases (0.03-4.6 kPa range, corresponding to the intrinsic sensitivity of the material) or to allow visual detection of the colour change (0.5 and 9.3 kPa range, for a significant conversion of the material) can be properly rationalized and determined. This study paves the way for quantification of MFC response to anisotropic forces at the macroscale and will be useful for applications in MFC-material-based mechanical stress probes. The approach reported herein is extremely promising to further investigate other families of MFC compounds and gain deeper insights in the MFC phenomenon.

Experimental section

The mechanical setup is made of: a linear motor Oriental Motor DRL60G-05B4M-KB, a rotation motor Oriental Motor AR46AK-H100-1, a force and torque sensor (or load cell) Futek MBA500 FSH00743, a 20 mm-diameter pestle, a CCD camera Retiga R3 equipped with an objective MVL7000 - 18-108 mm EFL, f/2.5 (with a filter Thorlabs FESH0700) and a silver mirror Thorlabs PFR14-P01 (25 mm x 36 mm x 1 mm). For all the shearing experiments, a piece of weakly auto-fluorescent paper is stuck on the pestle via double-sided tape in order to be rough enough to spread the analysed powder without scratching the glass. For pure compression experiments no paper is used to cover the pestle. The rotation rate was 0.3 RPM. In the case of a force ramp, vertical force was applied at a speed of 0.25 N/s. Movies are recorded via Ocular software in “Daylight” mode with an exposure time of 300 ms and one frame every 2 s. Vertical force and torque values are recorded via the in-house Agnes software of LMS every second.

Author Contributions

BP: investigation, data curation, formal analysis, visualization, validation, writing – original draft; ML: investigation, writing – review &editing; LB: conceptualization, methodology, software, writing – review &editing; RM: conceptualization, methodology,

visualization, writing – review &editing, supervision; CA: conceptualization, methodology, funding acquisition, writing – review &editing, supervision.

Conflicts of interest

There are no conflicts to declare.

Acknowledgements

This project has received funding from the European Research Council (ERC) under the European Union's Horizon 2020 research and innovation programme (grant agreement No 715757 MECHANO-FLUO to C. A.) and from the Mission pour l'Interdisciplinarité du CNRS (défi "Mécanobio"). L.B. acknowledges that this research benefited, through the use of the PLATINE platform, from the support of the École Polytechnique fund raising – Smart environments: Nanosensors and Nanoreliability Initiative. Erik Guimbretière, Pascal Marie and Vincent de Greef, at LMS, are acknowledged for respectively contributing to the design of the setup, machining the parts and adapting the Agnes software to the new setup.

References

1 J. Xu and Z. Chi, in *Mechanofluorochromic fluorescent materials: Phenomena, Materials and Applications*, eds. J. Xu and Z. Chi, Royal Society of Chemistry, Cambridge, 2014, pp. 1–6.
2 D. Yan and D. G. Evans, *Mater. Horiz.*, 2014, **1**, 46–57.
3 Y. Sagara, S. Yamane, M. Mitani, C. Weder and T. Kato, *Adv. Mater.*, 2016, **28**, 1073–1095.
4 C. Wang and Z. Li, *Mater. Chem. Front.*, 2017, **1**, 2174–2194.
5 Y. Sagara and T. Kato, *Nature Chem.*, 2009, **1**, 605–610.
6 M. Zhang, L. Zhao, R. Zhao, Z. Li, Y. Liu, Y. Duan and T. Han, *Spectrochim. Acta, Part A*, 2019, **220**, 117125.
7 P. Shi, D. Deng, C. He, L. Ji, Y. Duan, T. Han, B. Suo and W. Zou, *Dyes Pigm.*, 2020, **173**, 107884.
8 V. C. Wakchaure, T. Das and S. S. Babu, *ChemPlusChem*, 2019, **84**, 1253–1256.
9 S. K. B. Mane, Y. Mu, Z. Yang, E. Ubba, N. Shaishta and Z. Chi, *J. Mater. Chem. C*, 2019, **7**, 3522–3528.
10 D. Genovese, A. Aliprandi, E. A. Prasetyanto, M. Mauro, M. Hirtz, H. Fuchs, Y. Fujita, H. Uji-I, S. Lebedkin, M. Kappes and L. De Cola, *Adv. Funct. Mater.*, 2016, **26**, 5271–5278.
11 P. Shi, R. Zhao, M. Zhang, M. Lin, Y. Duan and T. Han, *Mater. Lett.*, 2019, **243**, 38–41.
12 Z. Chi, X. Zhang, B. Xu, X. Zhou, C. Ma, Y. Zhang, S. Liu and J. Xu, *Chem. Soc. Rev.*, 2012, **41**, 3878.
13 P. Xue, J. Ding, P. Wang and R. Lu, *J. Mater. Chem. C*, 2016, **4**, 6688–6706.
14 C. Calvino, L. Neumann, C. Weder and S. Schrettl, *J. Polym. Sci., Part A: Polym. Chem.*, 2017, **55**, 640–652.
15 A. Pucci, R. Bizzarri and G. Ruggeri, *Soft Matter*, 2011, **7**, 3689.
16 L. Polacchi, A. Brosseau, R. Métivier and C. Allain, *Chem. Commun.*, 2019, **55**, 14566–14569.
17 M. Louis, C. Piñero García, A. Brosseau, C. Allain and R. Métivier, *J. Phys. Chem. Lett.*, 2019, **10**, 4758–4762.
18 H. Kobayashi, S. Hirata and M. Vacha, *J. Phys. Chem. Lett.*, 2013, **4**, 2591–2596.
19 T. Nakamura and M. Vacha, *J. Phys. Chem. Lett.*, 2020, **11**, 3103–3110.
20 J. Wu, H. Wang, S. Xu and W. Xu, *J. Phys. Chem. A*, 2015, **119**, 1303–1308.
21 C. Feng, K. Wang, Y. Xu, L. Liu, B. Zou and P. Lu, *Chem. Commun.*, 2016, **52**, 3836–3839.
22 N. Li, Y. Gu, Y. Chen, L. Zhang, Q. Zeng, T. Geng, L. Wu, L. Jiang, G. Xiao, K. Wang and B. Zou, *J. Phys. Chem. C*, 2019, **123**, 6763–6767.
23 Q. Benito, B. Baptiste, A. Polian, L. Delbes, L. Martinelli, T. Gacoin, J.-P. Boilot and S. Perruchas, *Inorg. Chem.*, 2015, **54**, 9821–9825.
24 A. Makal, J. Krzeszczakowska and R. Gajda, *Molecules*, 2019, **24**, 1107.
25 Z. Fu, K. Wang and B. Zou, *Chin. Chem. Lett.*, 2019, **30**, 1883–1894.
26 L. Wang, K. Wang, B. Zou, K. Ye, H. Zhang and Y. Wang, *Adv. Mater.*, 2015, **27**, 2918–2922.
27 K. Nagura, S. Saito, H. Yusa, H. Yamawaki, H. Fujihisa, H. Sato, Y. Shimoikeda and S. Yamaguchi, *J. Am. Chem. Soc.*, 2013, **135**, 10322–10325.
28 Z. Man, Z. Lv, Z. Xu, Q. Liao, J. Liu, Y. Liu, L. Fu, M. Liu, S. Bai and H. Fu, *Adv. Funct. Mater.*, 2020, **30**, 2000105.
29 M. Sase, S. Yamaguchi, Y. Sagara, I. Yoshikawa, T. Mutai and K. Araki, *J. Mater. Chem.*, 2011, **21**, 8347.
30 M. Li, R. Tian, D. Yan, R. Liang, M. Wei, D. G. Evans and X. Duan, *Chem. Commun.*, 2016, **52**, 4663–4666.
31 T. Sagawa, F. Ito, A. Sakai, Y. Ogata, K. Tanaka and H. Ikeda, *Photochem. Photobiol. Sci.*, 2016, **15**, 420–430.
32 G. Zhang, J. Lu, M. Sabat and C. L. Fraser, *J. Am. Chem. Soc.*, 2010, **132**, 2160–2162.
33 T. Butler, M. Zhuang and C. L. Fraser, *J. Phys. Chem. C*, 2018, **122**, 19090–19099.
34 L. Wilbraham, M. Louis, D. Alberga, A. Brosseau, R. Guillot, F. Ito, F. Labat, R. Métivier, C. Allain and I. Ciofini, *Adv. Mater.*, 2018, **30**, 1800817.
35 A. Hakonen, J. E. Beves and N. Strömberg, *Analyst*, 2014, **139**, 3524–3527.
36 K. Cantrell, M. M. Erenas, I. de Orbe-Payá and L. F. Capitán-Vallvey, *Anal. Chem.*, 2010, **82**, 531–542.
37 Y. Wen, D. Kuang, J. Huang and Y. Zhang, *RSC Adv.*, 2017, **7**, 42339–42344.
38 J. Zhou, G. Lei, L. L. Zheng, P. F. Gao and C. Z. Huang, *Nanoscale*, 2016, **8**, 11467–11471.
39 A. Hakonen and J. E. Beves, *ACS Sens.*, 2018, **3**, 2061–2065.
40 A. Battisti, P. Minei, A. Pucci and R. Bizzarri, *Chem. Commun.*, 2017, **53**, 248–251.
41 J. Hou, X. Wu, W. Sun, Y. Duan, Y. Liu, T. Han and Z. Li, *Spectrochim. Acta, Part A*, 2019, **214**, 348–354.
42 J. Wu, Y. Cheng, J. Lan, D. Wu, S. Qian, L. Yan, Z. He, X. Li, K. Wang, B. Zou and J. You, *J. Am. Chem. Soc.*, 2016, **138**, 12803–12812.
43 G. R. Krishna, M. S. R. N. Kiran, C. L. Fraser, U. Ramamurty and C. M. Reddy, *Adv. Funct. Mater.*, 2013, **23**, 1422–1430.
44 G. R. Krishna, R. Devarapalli, R. Prusty, T. Liu, C. L. Fraser, U. Ramamurty and C. M. Reddy, *IUCrJ*, 2015, **2**, 611–619.

